Available online at www.sciencedirect.com
ScienceDirect
Biomedical Signal Processing and Control 2 (2007) 191–198
Biomedical Signal Processing and Control
www.elsevier.com/locate/bspc

Needle insertions modeling: Identifiability and limitations

L. Barbé [a,*], B. Bayle [a], M. de Mathelin [a], A. Gangi [b]

[a] LSIIT, UMR CNRS 7005, Bld Sébastien Brant, F-67400 Illkirch, France
[b] Radiology Department B, University Hospitals of Strasbourg, 67091 Strasbourg, France

Received 28 February 2007; received in revised form 30 May 2007; accepted 4 June 2007
Available online 7 August 2007

Abstract

Soft tissues modeling is a very present preoccupation in different scientific fields, from computer simulation to biomechanics or medical robotics. In this article, we consider the interaction of a needle with living tissues, which is a particularly complex modeling problem since it is characterized by inhomogeneity and nonlinearity properties. We propose a robust method to online estimate forces involved in typical percutaneous interventions. The ability to obtain physically consistent models during *in vivo* insertions is also discussed.

Keywords: Soft tissues modeling; Online robust estimation; Interventional radiology

1. Introduction

Percutaneous needle insertions are among the most common procedures in medicine. They probably represent the least invasive way to directly reach internal zones of a body. Additionally to the classical subcutaneous injections, they have also developed in surgery and interventional radiology. In these domains, the corresponding medical treatments range from simple biopsies to radiofrequency ablation of cancers, typically in the liver.

For a few years, the modeling of the interaction forces during needle insertions has become a challenging task. This research effort has been motivated by the development of simulators, which help unexperienced clinicians to learn needle insertion procedures, and by the development of robotic systems to assist percutaneous interventions [19,20]. In this context, pioneer modeling works recently appeared, principally in the medical robotics context [5,17] and a first paper proposed a review of the domain [1].

1.1. Needle insertion description

To characterize the interaction between a needle and soft living tissues, let us first describe a puncture into a single layer sample. We assume that the needle tip is initially motionless, in contact with the surface of the tissue. The needle insertion is a 3-phase procedure illustrated by Fig. 1:

- Phase 1: The needle pushes the tissue surface which becomes deformed.
- Phase 2: When the force applied by the needle on the tissue reaches a given energetic threshold [9], the needle penetrates into the tissue by cutting its surface. While the needle is inserted, the friction forces attract the skin along the needle shaft.
- Phase 3: The needle is extracted from the tissue. Again, the tissue is attracted in the needle motion direction. Then, the position of the needle when it is extracted is different from the initial position.

The first phase corresponds to a viscoelastic interaction as described by Fung [7]. According to Okamura et al. [17] the interaction forces during the second phase result from the combined effects of cutting and friction and from the relaxation of the skin after the puncture. During the third phase, the interaction between the needle and the tissue is only due to

* Corresponding author.
E-mail addresses: barbe@eavr.u-strasbg.fr (L. Barbé), bernard@eavr.u-strasbg.fr (B. Bayle), demath@eavr.u-strasbg.fr (M. de Mathelin).

1746-8094/$ – see front matter © 2007 Elsevier Ltd. All rights reserved.
doi:10.1016/j.bspc.2007.06.003

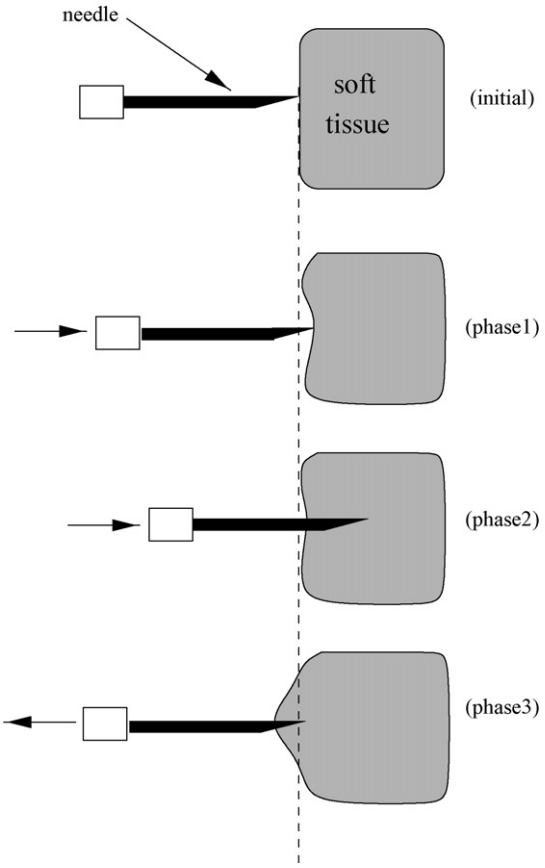

Fig. 1. Needle insertion into a single layer soft tissue.

friction. It is particularly difficult to characterize the insertion in living tissues because:

- the different tissues in interaction with the needle are inhomogeneous;
- these tissues exhibit nonlinear properties;
- their contributions to the interaction are superimposed.

Fig. 2 shows the force profile during a typical needle insertion. The insertion is performed directly into the liver of a living pig and

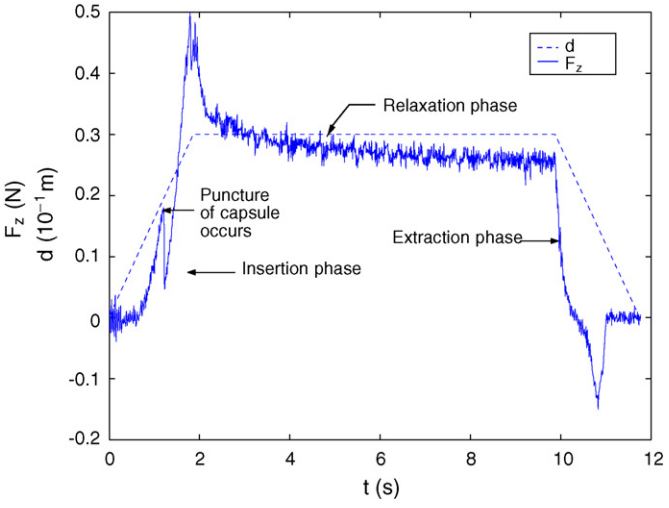

Fig. 2. Force profile during a robotized needle insertion into the liver [16].

the motion of the needle holder is controlled by a robotic system [16]. The discontinuity in the force profile during the insertion corresponds to the rupture of the hepatic membrane. In ref, [16], we use existing models to characterize the insertion phase. However, the hepatic membrane puncture is not considered, as this would require to know or detect the rupture time.

1.2. Needle insertion modeling

Okamura et al. [17] study the forces involved in the penetration and the withdrawal of a needle into a piece of bovine liver. The main contribution of the paper is to describe needle insertion mechanics and to propose a methodology to separate the contributions of stiffness, friction and cutting forces, in order to derive a complete force model. Though the proposed method is suitable for the characterization of efforts and for simulation, it involves different specific *ex vivo* tests to adjust parameters to patient variability. The rheological characterization of tissues, proposed in ref. [14] has the same limitations.

During an intervention, the insertion of the needle into a patient has to be limited to the necessary medical act. Therefore, the identification of a needle insertion model, in order to use it in per-operative conditions, has to be performed with the data collected during the medical act itself. DiMaio and Salcudean [5] estimate an elastostatic linear model derived from the needle tip force and position measurements and from the deformation of the pierced material. As the deformations are given by markers placed on the surface of the material, this procedure does not easily apply in clinical conditions, specially in the case of internal organs. In the context of the interaction of a robot with a soft environment, Diolaiti et al. [6] focus on the online estimation of viscoelastic linear and nonlinear models. The proposed methodology is of interest though results are given for small motions of a translator system in contact with thin layers of stiff (polycarbonate) and soft (silicone gel) samples. Since experiments are performed with artificial materials and viscoelastic stimuli, *i.e.* without cutting, the method does not directly adapt to the problem of needle insertion. Nevertheless, this approach shares similar motivations with our study.

1.3. Contributions and outline

In this article, we analyze the modeling and the identification of needle insertion interactions during *in vivo* experiments. The limitations of the proposed modeling are discussed throughout the text. In section 2, the experimental setup and the estimation techniques are presented. Section 3 deals with the modeling issues and the results of online estimations obtained during *in vivo* experiments. Finally, the conclusion summarizes the main contributions of this work.

2. Methods

2.1. Experimental setup

As already stated, the aim of this paper is to model the forces involved during the needle insertion from measurable

informations in operating conditions. We consider that the tissues in which the needle is inserted are not equipped with particular fiducials that may allow to capture the organs motions. We suppose that the only informations at disposal are the position or the velocity of the needle tip and the interaction forces measured by a force sensor.

To estimate needle insertion models we use a PHANToM haptic device from Sensable Technologies as an instrumented passive needle holder (see Fig. 3). Its encoders allow to measure the motions of the needle with a precision of 30 μm. The PHANToM end effector is equipped with an ATI Nano17 force sensor. All measurements are acquired at a frequency rate of 1 kHz, under real-time constraints imposed by the software implemented on Linux RTAI operating system. Finally, a needle holder is mounted on the force sensor so that needles of different sizes can be attached. Nevertheless, in the following experiments we will always use a 18-Gauge needle. For more details on the effect of the needle size and of its geometry, see [17] or [1].

During a manual insertion, the velocity of the needle tip is generally very low. Since it is derived from position encoders, it is corrupted by an important quantization noise. To reduce the perturbations induced by this noise in the model, the estimation of the velocity has been obtained by a Kalman filter. The equations of this Kalman filter are based on an estimation of the velocity v_k and the position p_k of the needle tip:

$$p_{k+1} = p_k + Tv_k + \frac{T^2}{2}\gamma_k, \qquad v_{k+1} = v_k + T\gamma_k \tag{1}$$

where T is the sampling period and γ_k is a noise signal that represents the unknown acceleration of the needle. This latter is considered as a white noise with variance $q = E\{\gamma_k^2\} = d/T^2$, where d is the position accuracy [3]. We can derive a state model from Eq. (1) by choosing $x_k = (p_k\ v_k)^{\mathrm{T}}$ as the state vector. Then $y_k = p_k + w_k$ is the measurement equation, with w_k the measurement noise. We assume that $-d \le w_k \le d$ and that w_k has a zero mean value bounded uniform distribution, that leads to the variance $r = E\{w_k^2\} = d^2/3$ [12]. The state model from Eq. (1) is then:

$$x_{k+1} = A_k x_k + G_k\gamma_k, \qquad y_k = C_k x_k + w_k$$

with:

$$A_k = \begin{pmatrix} 1 & T \\ 0 & 1 \end{pmatrix}, \quad G_k = \begin{pmatrix} \frac{T^2}{2} \\ T \end{pmatrix}, \quad C_k = (1 \quad 0)$$

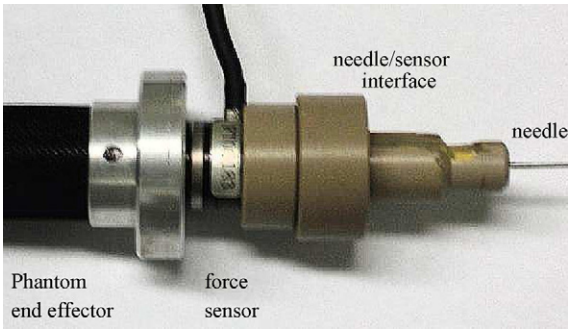

Fig. 3. Instrumented needle.

The Kalman filter algorithm is then applied for state estimation [12]:

$$K_k = P_k C_k^{\mathrm{T}}(r + C_k P_k C_k^{\mathrm{T}})^{-1},$$

$$\hat{x}_{k+1} = A_k\hat{x}_k + A_k K_k(y_k - C_k\hat{x}_k),$$

$$P_{k+1} = A_k(I - K_k C_k)P_k A_k^{\mathrm{T}} + qG_k G_k^{\mathrm{T}}$$

with the initial values $K_0 = (0 \quad 0)^{\mathrm{T}}$, $\hat{x}_0 = (0 \quad 0)^{\mathrm{T}}$ and

$$P_0 = \begin{pmatrix} \frac{d^2}{3} & 0 \\ 0 & \frac{2d^2}{3T^2} \end{pmatrix}.$$

2.2. Online estimation method

We use a recursive estimation method in order to identify a model of forces due to the interaction between the needle and the tissue. This method is based on *a priori* models, that will further be discussed.

2.2.1. Problem formulation

Recursive parametric estimation algorithms [8] are based on a discrete time linear parameterization of the system:

$$y_{k+1} = \varphi_k^{\mathrm{T}}\theta_k^* \tag{2}$$

where θ_k^* is the vector of unknown parameters to be estimated, φ_k the regression vector built from measured signals and y_k is the measured output signal.

Using the estimation $\hat{\theta}_k$ of θ_k^*, at time k, the output signal at time $k+1$ can be predicted as:

$$\hat{y}_{k+1} = \varphi_k^{\mathrm{T}}\hat{\theta}_k \tag{3}$$

The *a priori* prediction error is defined as the error between the measured output and the predicted output:

$$e_{k+1} = y_{k+1} - \hat{y}_{k+1} = \varphi_k^{\mathrm{T}}(\theta_k^* - \hat{\theta}_k)$$

Finally, we define the *a posteriori* prediction error:

$$\hat{e}_{k+1} = y_{k+1} - \varphi_k^{\mathrm{T}}\hat{\theta}_{k+1} = \varphi_k^{\mathrm{T}}(\theta_k^* - \hat{\theta}_{k+1})$$

2.2.2. Robust recursive least squares

The Recursive Least Squares (RLS) algorithm is probably the most used technique for online estimation. The basic RLS algorithm can be written as:

$$\begin{aligned} \hat{\theta}_k &= \hat{\theta}_{k-1} + \frac{F_{k-1}\varphi_{k-1}e_k}{(1/(\alpha_{k-1})) + \varphi_{k-1}^{\mathrm{T}}F_{k-1}\varphi_{k-1}}, \\ F_k &= F_{k-1} - \frac{F_{k-1}\varphi_{k-1}\varphi_{k-1}^{\mathrm{T}}F_{k-1}}{(1/(\alpha_{k-1})) + \varphi_{k-1}^{\mathrm{T}}F_{k-1}\varphi_{k-1}} \end{aligned} \tag{4}$$

where α_k is a weighting function. In the basic RLS algorithm $\alpha_k = 1$. It can be chosen as the inverse of the expected mean-square error [8] to attach a smaller weight to the terms for which y_k is expected to have a larger error.

Additionally to the standard algorithm it is recommended to use a dead-zone function [4,11] so that the RLS estimation may remain robust to noise when the absolute value of the error signal is under a given threshold, denoted by N_0 and chosen such that $N_0 > v_0$, with v_0 a bound on the magnitude of the output noise. The resulting RLS algorithm is obtained by premultiplying F_k by $\delta(e_k)$, with:

$$\delta(e_k) = \begin{cases} 1, & \text{if } |e_k| \geq 2N_0 \\ \dfrac{|e_k|}{N_0} - 1, & \text{if } N_0 \leq |e_k| < 2N_0 \\ 0, & \text{if } |e_k| < N_0 \end{cases} \quad (5)$$

When the error is small, a noticeable robustness improvement results from the freezing of the parameters adaptation.

2.2.3. Estimation of varying parameters

In the RLS algorithm, the gain factor F_k is not constant. This has some influence on the estimation of varying parameters. Indeed, a persisting excitation of the regression vector, i.e. a sufficient level of richness of the input measurements, is required for the convergence of the parameters estimates to their values. In the case of the standard RLS method, the convergence of the algorithm causes the decrease of F_k to zero and, consequently, the estimated parameters no longer vary, so that the estimation of time-varying parameters is not possible. The RLS algorithm with covariance resetting (RLS-CR) solves the problem of the decrease of the adaption gain by a resetting of the covariance matrix [8]. This resetting is performed at time k_r with:

$$\{k_r\} = \{k | \lambda_{\min}(F_k) \leq \alpha_0^{-1} \leq \lambda_{\min}(F_{k-1})\}$$

with $\lambda_{\min}(F_k)$ the minimal eigenvalue of matrix F_k. To reduce the computing complexity of k_r, an equivalent condition on the trace of the covariance matrix can be used:

$$\{k_r\} = \{k | x_k = \mathrm{tr}(F_k^{-1}) \geq \alpha_0\}$$

Indeed, it was shown [8] that x_k can be computed recursively by:

$$x_k = x_{k-1} + \alpha_{k-1} \varphi_{k-1}^{\mathrm{T}} \varphi_{k-1}$$

The resetting, at the time k_r, is then achieved by setting $F_{k_r} = F_0$, which also implies $x_{k_r} = x_0 = \mathrm{tr}(F_0^{-1})$.

3. *In vivo* experimental results

We led two different tests.

Firstly, we identified the viscoelastic behavior of the tissues that occurs in the first phase of the insertion (see Fig. 1). Since no piercing was necessary, we performed the test on the abdomen of an adult living human. The final part of the needle holder was removed and the force sensor mounted on the end effector directly applied on the abdomen. The corresponding results are given in Section 3.1.

The second part of the experiments were performed in operating *in vivo* conditions. Needle insertions in the liver of anesthetized pigs were adopted as benchmarks for two reasons:

- the abdominal tissues of a young pig are rather similar to human ones;
- the properties of the tissues are much more realistic *in vivo* because of blood irrigation and breathing which considerably influence the mechanical properties of the tissues.

The insertion was done through a small incision on the epidermis (a new one each time), as usually done in interventional radiology. The insertion was then performed through the dermis, the fat and the muscle to finally access the liver. The corresponding results are given in Section 3.2.

3.1. Viscoelastic experiments

3.1.1. Modeling

To model the interaction during the viscoelastic phase of the needle insertion, we considered two classical viscoelastic models. The linear Kelvin–Voigt (KV) model is certainly the most common model used in the literature [7]. It corresponds to a spring-damper model, as illustrated by Fig. 4.

In our case is written as:

$$f = \begin{cases} -(Kp + Bv), & \text{if } p > 0 \\ 0, & \text{if } p \leq 0 \end{cases} \quad (6)$$

where f is the force exerted by the tissue on the needle, p and v represent the position and the velocity of the needle tip, K is the stiffness coefficient and B the damping coefficient. The position $p = 0$ corresponds to the initial contact point. In fact, the representation of living tissues by this linear model is generally not adequate. Indeed, except for very small motions the interaction model varies in an nonlinear way regardless to the tissue motion. The Hunt-Crossley (HC) model intrinsically takes into account the penetration depth between two bodies. It states that the interaction model varies in a nonlinear way regardless to the tissue motion, as presented in [10]:

$$f = \begin{cases} -(\mu p^n + \lambda p^n v), & \text{if } p > 0 \\ 0, & \text{if } p \leq 0 \end{cases} \quad (7)$$

where μ, λ and n are constant parameters that depend on the material properties.

Table 1 gives the definition of each variable for the recursive estimation algorithms, in the case of the KV and HC models (discrete time representation).

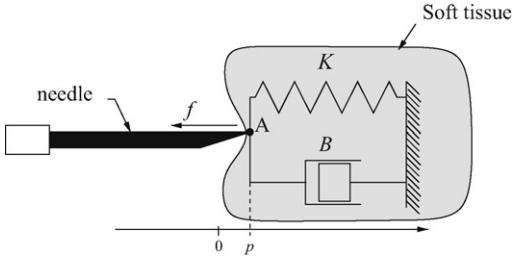

Fig. 4. Representation of the Kelvin–Voigt model.

Table 1
Definition of the variables for the KV and the HC model

Variables	KV model	HC model
φ_k^{T}	$(p_k\ v_k)$	$(p_k^n\ p_k^n v_k)$
$\theta_k^{*\mathrm{T}}$	$(K_k\ B_k)$	$(\mu_k\ \lambda_k)$
y_k	f_k	f_k
$\hat{y}_k$	$\hat{f}_k$	$\hat{f}_k$

3.1.2. Experimental results

From the previous remarks, and from comparative tests between the KV and HC models, we used the HC model for the estimation in the viscoelastic case. Characteristic results are presented in Fig. 5. This figure illustrates the quality of the force reconstruction. Force is given as a function of the needle tip position. This allows to emphasize the nonlinearity of the model. The absolute mean value of the reconstruction error is 0.0194 N, with a standard deviation of 0.0125 N.

The HC model allows to obtain quasi constant parameters during the viscoelastic interaction as illustrated in Fig. 6. We observe the convergence of the algorithm to $\mu = 240$ and $\lambda = 1.5$. In that study we assumed that the n coefficient is constant, which is generally the case in the biomechanics literature. According to [13], $n \simeq 1.5$ in the case of spheres contacting in static conditions. [6] establish that $n \simeq 1.3$ describes accurately the viscoelastic behavior of soft materials. The authors also propose a solution for the simultaneous online estimation of μ, λ and n. In our experiments, we selected $n = 1.3$.

Remarks. According to Fung [7] most living tissues have a viscoelastic behavior, as long as small displacements are considered. In practice, we could observe that the viscoelastic phase during a needle insertion corresponds to relatively large motions. This increases the nonlinear behavior of the tissue. We could also observe an even more disturbing artifact. When the needle is inserted in very viscous organs, they trend to slip in the abdominal cavity. This of course is very difficult to model. In practice, it is avoided by the physician, which often tries to minimize the viscoelastic phase of the insertion by piercing the organs with an abrupt motion of the needle [9].

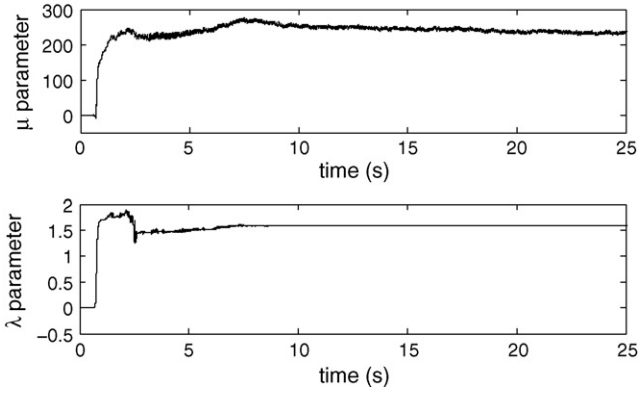

Fig. 6. Estimated parameters of the HC model during the viscoelastic phase.

3.2. Needle insertion experiments

3.2.1. Modeling

For clarity purpose, we consider the simple case of the insertion of a needle into a one layer soft tissue. As underlined previously, the behavior of the tissue during the first phase of the insertion (see Fig. 1) can be approximated by a viscoelastic model. So, if the position of the entry point on the surface of the tissue is denoted by p_s, the motion of the tissue can be described by : $p = p_s$, as represented in Fig. 7. During this phase, the tissue surface is deformed until the penetration of the needle tip. The measured force can be expressed by either the KV or the HC model. The HC model is probably the most suitable, as the tissue deformation is often important. With this model, if the speed is relatively slow $f \simeq -\mu p^n$, which corresponds to a polynomial force profile as mentioned in [17,16].

After the puncture, the needle tip position is different from the position of the entry point on the surface of the tissue (see Fig. 7). Then, it is much more difficult to express f, than in the simple viscoelastic case. In the case of the liver, [17] assume

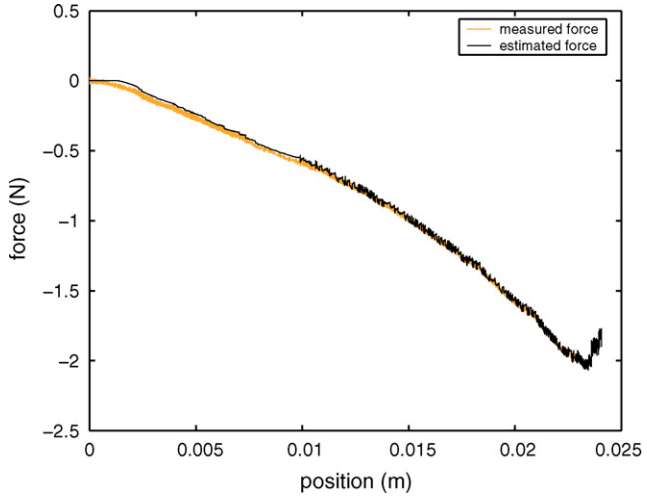

Fig. 5. Force reconstruction with the HC model during the viscoelastic phase.

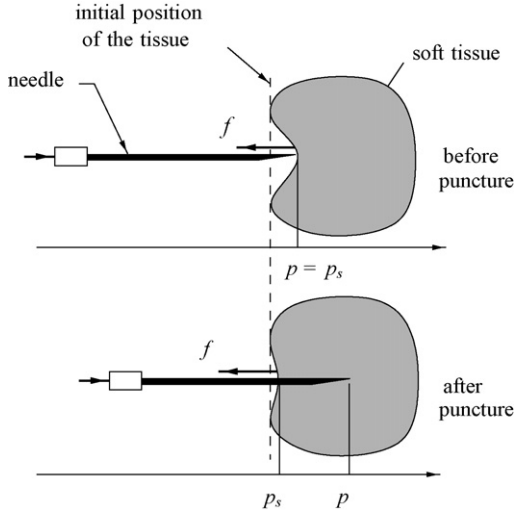

Fig. 7. Description of the needle insertion.

that after the liver capsule puncture, the measured force is composed of a friction force and a cutting force. This latter term, which is dominant in the results of [17], is a combination of the actual cutting force and of the stiffness force due to the persisting tissue compression. Indeed, whereas friction is identified by periodic stimuli of liver samples, it remains difficult to separate the contribution of cutting and stiffness.

Based on the HC model for the viscoelastic terms, we can express the total insertion force on the needle as:

$$f = -\mu p_s^n - \lambda p_s^n(v_s - v) + f_f + f_c$$

where $v_s = \dot{p}_s$, f_f is the dry friction force on the needle shaft, and f_c the cutting force applied on the needle bevel. Note that the values of μ and λ are different from that of the viscoelastic phase, since the interaction conditions changed. With such a refinement in the model, it is, however, extremely difficult to identify the different parameters. Additionally, as we aim at making this identification without markers on the skin p_s will remain unknown. So the precise estimation of such a model is definitively out of reach.

A first solution consists in grouping some of the terms of the model as proposed by [17]. Another possibility is to use a simpler but less accurate model. Yen et al. [21] propose a model of tissue for needle insertion based on a KV model with piecewise constant parameters. Since the needle punctures several inhomogeneous layers that all have different behaviors, this appears quite sensible. However, the difficulty is to detect the organs transitions instants or finer details like, for instance, small vessels ruptures. Finally, as the force model during the whole procedure cannot be described by constant parameters, neither for the KV model nor for the HC, we decided to use the simplest model, that is a model in the KV form, but for which the parameters K and B are time-varying and depend on the position and the velocity of the needle tip, i.e., such that:

$$\begin{cases} K = K(p, v, t) \\ B = B(p, v, t) \end{cases}$$

In the following we will denote this model as the KV Generalized (KVG) model.

It is necessary to remark that the proposed model cannot be considered rigorously as physically accurate, since it does not take into account the tissues deformations, the friction or the cutting. It means that the K and B parameters are no longer rigorously stiffness and viscous friction coefficients.

3.2.2. Experimental results during a needle insertion directly into the liver

In this case, the results obtained for the force reconstruction are represented in Fig. 8. This figure shows the measured force profile compared to the force reconstruction on the one hand (top) and the error of force reconstruction on the other hand (bottom). The estimation results in Fig. 8 are very accurate: the absolute error mean value is 32.2 mN, for a force amplitude ranging from −1.48 to 0.69 N. Two punctures appear on the force profile during the insertion. The first one corresponds to the hepatic membrane rupture and the second one is probably due to the presence of a large vein. The needle is extracted just after the end of the insertion, at time $t = 4.5$ s and thus no relaxation phase is observed.

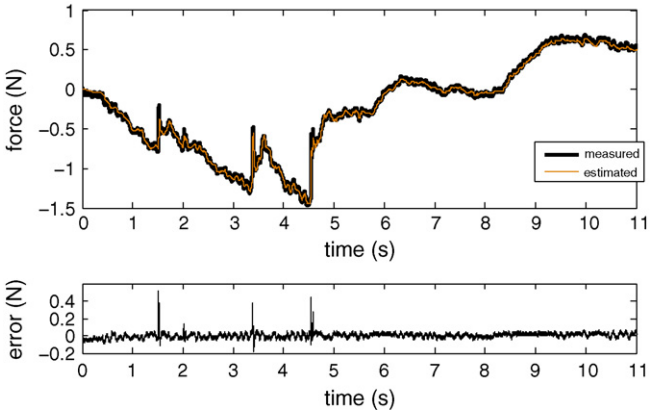

Fig. 8. Force reconstruction with the KVG model during a needle insertion directly into the liver.

The evolution of the estimated parameters of the KVG model during the needle insertion is represented in Fig. 9. After the delay required for the algorithm convergence, the B parameter is approximately constant during both the insertion and the extraction of the needle. The evolution of the K parameter looks like a piecewise constant function, whose discontinuities are determined by the position of the ruptures during the insertion.

This observation corresponds to the model proposed by [21]. However, remark that in our procedure the parameters changes are automatic and not *a priori* chosen, as functions of the needle tip depth. This is a noticeable improvement over [21] work.

3.2.3. Experimental results during a needle insertion into the liver through the skin

In this case, i.e. through the skin, the results obtained for the force reconstruction are represented in Fig. 10. Again, the limited reconstruction error proves the accuracy of the method: the absolute error mean value is 25.3 mN for a force amplitude ranging from −5.69 to 2.45 N. The increase in the force range emphasizes the fact that most of the forces that a physician feels while inserting a needle are due to the skin, the fat and the muscles.

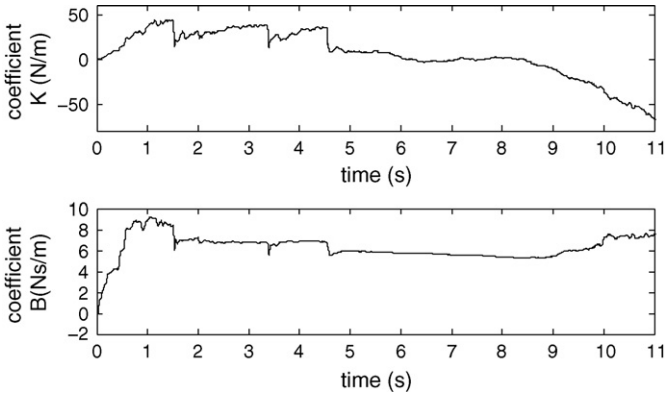

Fig. 9. Estimated parameters of the KVG model during a needle insertion directly into the liver.

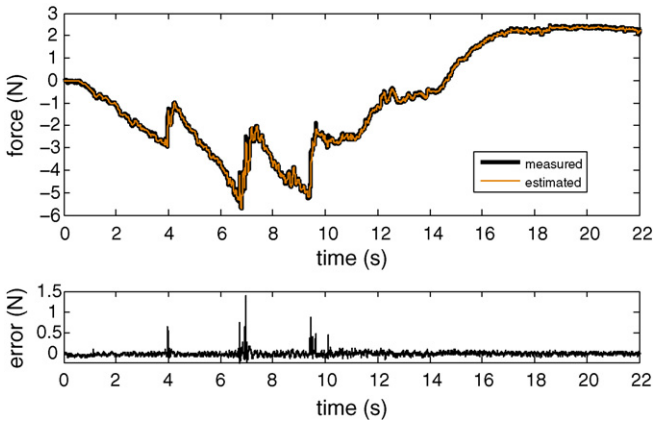

Fig. 10. Force reconstruction with the KVG model during a needle insertion.

The main interest of this model is related to the parameters analysis. The evolution of the estimated parameters of the KVG model during the needle insertion are represented in Fig. 11. The profile of both parameters of the KVG model are not continuous, because of the rupture of the different tissues surfaces. The profile of parameter B is quite similar to the one of the needle insertion directly into the liver, but we can notice that the transitions phases are more significant. The transition phases are also very present in the evolution of the K parameter. The amplitude of K is greater than in the insertion directly into the liver, and it is more dependent on the needle tip position. Nevertheless, we notice that the parameters are bounded and fluctuate slowly excepted during transitions phases. This may open opportunities in the control of robotized needle insertion systems.

Remarks. On the one hand, we can remark that during both the insertions presented in this section, it is hardly possible to distinguish the measured and the estimated forces. In fact, the most important errors happen during fast changes in the force signal. During more stationary periods, the RLS-CR scheme offers a very accurate reconstruction. This is illustrated by Fig. 12, which represents these two situations. Both the proposed plots are magnifications of Fig. 10. In the top plot, the measured force signal together with its estimate are represented between $t = 1.5$ s and $t = 2.5$ s, which corresponds to an

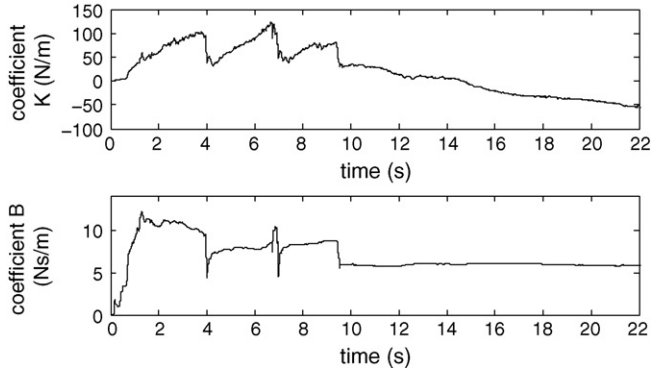

Fig. 11. Estimated parameters of the KVG model during a needle insertion.

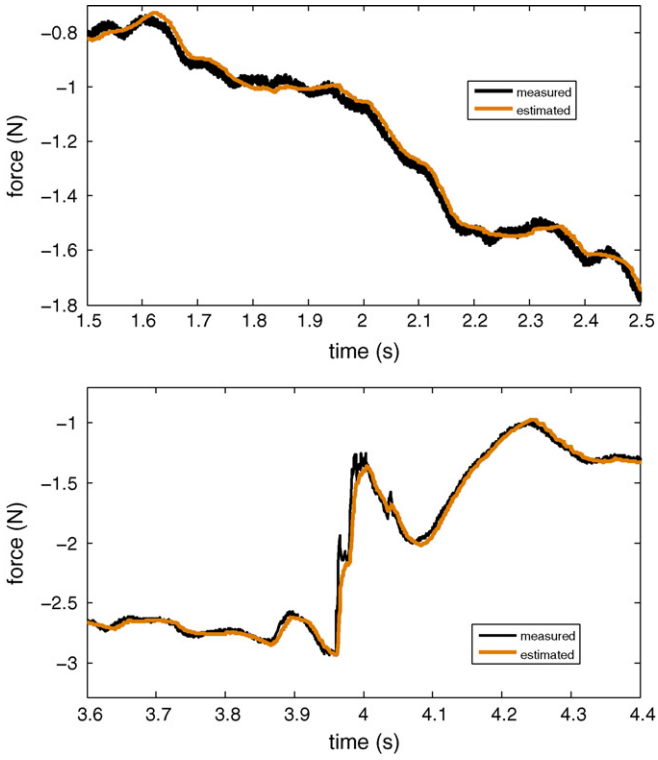

Fig. 12. Force reconstruction with the KVG model: steady state (top), transition (bottom).

insertion into homogeneous structures. In the bottom plot, the same signals are represented between $t = 3.8$ s and $t = 4.15$ s, when the rupture of a membrane happens, provoking a fast variation in the force signal. We can remark that, in spite of an non negligible transient error, the estimation algorithm fast converges again to the actual measured force.

On the other hand, Figs. 8 and 10 of Section 3.2 both correspond to the plot of the force exerted by the needle as a function of time. As theoretical models give the dependence of the force with respect to the needle tip position and velocity, it is also interesting to consider force as a function of position, as we did in Section 3.1. However, this plot is cyclic because of to the successive insertion and extraction of the needle. The resulting characteristics is then less simple to understand and analyze,

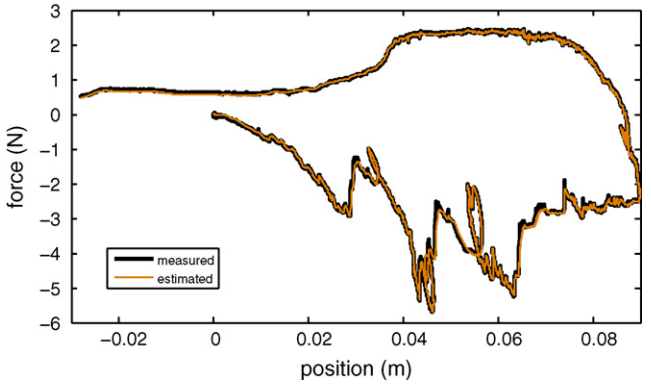

Fig. 13. Force reconstruction with the KVG model, during a needle insertion; force is plotted with respect to the needle tip position.

which justifies the presentation in Section 3.2. To illustrate this phenomenon, Fig. 13 represents the measured and estimated forces as functions of the needle tip position, in the case of the needle puncture into the liver, through the skin. They correspond to the measured and estimated forces previously represented in Fig. 10, as functions of time.

4. Conclusion

In this paper, we have presented a method to online characterize needle insertions. It is based on a robust recursive least squares algorithm with covariance resetting, which was selected for its efficiency, its robustness and its fast adaptation to parameters changes. A set of experiments allowed to evaluate the viscoelastic behavior of the skin and to prove the effectiveness of the estimation technique with classical viscoelastic models. Then, the insertion of a needle was described and the complex behavior of the tissues emphasized. For the online estimation of the needle insertion we proposed a varying parameters model. From this model, we could achieved the *in vivo* estimation of the needle interactions with very good tracking properties.

From the experimental results we can conclude that a model with piecewise constant parameters depending on the position and the velocity of the needle enables a good simple biomechanical description of the different tissues crossed by the needle. A possible extension of this work would be to incorporate friction terms in the estimated model, so as to improve its physical interpretation.

Concerning the exploitation of these results, the estimation procedure will further be introduced in the control of a force feedback teleoperation scheme, as suggested in ref. [2]. It will finally be implemented in a robotic assistant for percutaneous procedures, presently under prototyping [15,18].

Acknowledgements

This work has been supported by the Alsace Regional Council and the French National Center for Scientific Research (CNRS). The authors would like to thank the IRCAD/EITS staff for their help in arranging ideal surgical facilities, with a special thanks to Antonello and Stefano for their assistance during surgical acts.

References

[1] N. Abolhassani, R. Patel, M. Moallem, Needle insertion into soft tissue: A survey, Med. Eng. Phys. 29 (2007) 413–431.
[2] L. Barbé, B. Bayle, M. de Mathelin, Bilateral controllers for teleoperated percutaneous interventions: evaluation and improvements, in: American Control Conference, Minneapolis, USA, 2006.
[3] P. Bélanger, Estimation of angular velocity and acceleration from shaft encoder measurements, in: IEEE International Conference on Robotics and Automation, Nice, France, (1992), pp. 585–592.
[4] M. de Mathelin, in: R. Lozano, D. Taoutaou (Eds.), Commande adaptative et applications. Chap. Panorama des algorithmes récursifs d'estimation paramétrique, Hermès Science, 2001 (in French).
[5] S. DiMaio, S. Salcudean, Needle insertion modeling and simulation, IEEE Trans. Robot. Automat. 5 (19) (2003) 864–875.
[6] N. Diolaiti, C. Melchiorri, S. Stramigioli, Contact impedance estimation for robotic systems, IEEE Trans. Robot. 21 (5) (2005) 925–935.
[7] Y.C. Fung, Biomechanics: Mechanical Properties of Living Tissues, Springer-Verlag, 1993.
[8] G. Goodwin, K.S. Sin, Adaptive Filtering Prediction and Control. Information and System Sciences, Prentice-Hall, 1984.
[9] M. Heverly, P. Dupont, J. Triedman, Trajectory optimization for dynamic needle insertion, in: IEEE International Conference on Robotics and Automation, Barcelona, Spain, (2005), pp. 1658–1663.
[10] K. Hunt, F. Crossley, Coefficient of restitution interpreted as damping in vibroimpact, ASME J. Appl. Mech. (1975) 440–445.
[11] P. Ioannou, J. Sun, Robust Adaptive Control, Prentice-Hall, 1996.
[12] F. Janabi-Sharifi, V. Hayward, C-S.J. Chen, Discrete-time adaptive windowing for velocity estimation, IEEE Transactions on Control Systems Technology 8 (6) (2000) 1003–1009.
[13] K.L. Johnson, Contact Mechanics, Cambridge University Press, 1989.
[14] Y. Kobayashi, J. Okamoto, M.G. Fujie, Physical properties of the liver for needle insertion control, in: IEEE/RSJ International Conference on Intelligent Robots and Systems, Sendai, Japan, (2004), pp. 2960–2966.
[15] B. Maurin, J. Gangloff, B. Bayle, M. de Mathelin, O. Piccin, P. Zanne, C. Doignon, L. Soler, A. Gangi, A parallel robotic system with force sensors for percutaneous procedures under CT-guidance, in: International Conference on Medical Image Computing and Computer Assisted Intervention, Saint-Malo, France, (2004), pp. 176–183.
[16] B. Maurin, L. Barbé, B. Bayle, P. Zanne, J. Gangloff, M. de Mathelin, A. Gangi, A. Forgionne, In vivo study of forces during needle insertions, in: Scientific Workshop on Medical Robotics, Navigation and Visualization, Remagen, Germany, (2004), pp. 415–422.
[17] A. Okamura, C. Simone, M. O'Leary, Force modeling for needle insertion into soft tissue, IEEE Trans. Biomed. Eng. 51 (10) (2004) 1707–1716.
[18] O. Piccin, P. Renaud, L. Barbé, B. Bayle, B. Maurin, M. de Mathelin, A robotized needle insertion device for percutaneous procedures, in: ASME Design Engineering Technical Conferences, Long Beach, USA, 2005.
[19] D. Stoianovici, J. Cadeddu, R. Demaree, H. Basile, R. Taylor, L. Whitcomb, L. Kavoussi, A novel mechanical transmission applied to percutaneous renal access, ASME Dynam. Syst. Control Div. 61 (1997) 401–406.
[20] J. Yanoff, J. Haaga, P. Kalhr, C. Bauer, D. Nakamoto, A. Chaturvedi, R. Bruce, Ct-integrated robot for interventional procedures: preliminary experiment and computer-human interfaces, Comput. Aided Surg. 6 (6) (2001) 352–359.
[21] P.-L. Yen, R. Hibberd, B. Davies, A telemanipulator system as an assistant and training tool for penetrating soft tissue, Mechatronics 6 (4) (1996) 423–436.